Parolai, S., Bindi, D., Ullah, S., Orunbaev, S., Usupaev, S., Moldobekov, B., Echtler, H. (2013): The Bishkek vertical array (BIVA): acquiring strong motion data in Kyrgyzstan and first results. - Journal of Seismology, 17, 2, 707-719

DOI: 10.1007/s10950-012-9347-y

The Bishkek Vertical Array (BIVA): acquiring strong motion data in Kyrgyzstan and first results.

S. Parolai[1,*], D. Bindi[1], S. Ullah[1], S. Orunbaev[2], S. Usupaev[2], B. Moldobekov[2], H. Echtler[1].

[1]Deutsches GeoForschungsZentrum GFZ, Helmholtzstrasse 7, 14467 Potsdam, Germany.

[2] Central Asian Institute for Applied Geosciences Timur Frunze rd.73/2 720027 Bishkek, Kyrgyz Republic

*Corresponding author: Helmholtz Centre Potsdam, GFZ German Research Centre for Geosciences, Centre for Early Warning, Helmholtzstrasse 7, H7 103, 14467 Potsdam, Germany. Tel.:+493312881290, fax: +493312881204, E-mail: parolai@gfz-potsdam.de

Abstract

We present results from a vertical array of accelerometers that was recently installed in Bishkek (Kyrgyzstan) with the long-term aim of recording strong motion data. Taking advantage of recordings of a Mb 4.7 earthquake that occurred 40 km from the array site during the installation phase, we provide results of some preliminary data analysis. First, estimates of the S-wave velocity and Qs structure are deduced by the inversion of the deconvolved wavefield between the sensors in the borehole. Furthermore, the application of the nonstationary ray decomposition (Kinoshita, 2009) allowed at least 3 reflectors in the shallow velocity structure below the array to be identified. The complex nature of the wavefield (with upgoing, down-going waves, and converted phases) due to the coarse, unconsolidated subsoil structure is highlighted by means of numerical simulations of ground motion.

1. INTRODUCTION

The city of Bishkek (the capital of Kyrgyzstan) is located in one of the highest seismic hazard areas of the world (Zhang *et al*., 1999) directly adjacent to the active orogenic front of the Northern Tien Shan ridge. Recent seismic risk assessment studies (e.g., Erdik *et al*., 2005; Bindi *et al*., 2011) have shown that due to the high vulnerability of the building stock, very high direct losses (human and economic) would be expected in the case of a plausible event in the seismically active zones around the city.

Unfortunately, both the probabilistic seismic hazard assessment and the seismic hazard scenarios calculated for this area suffer from a lack of local strong ground motion data, and in particular, the behavior of the thick unsorted alluvial sediments underlying Bishkek during strong ground shaking can only be guessed at (Parolai *et al*., 2010 and references therein). Parolai *et al.* (2010) showed that site amplification is significant over a wide frequency band and that it varies across different parts of the town. They also showed, on the basis of seismic noise measurements, that the shear wave velocity ranges between 500 and 600 m/s in the shallowest few tens of meters in the coarse conglomerates, and that therefore the large observed amplifications are a result of strong impedance contrasts at depths of hundreds to a few thousands of meters (the crystalline basement depth is expected to be about 3000 m below the site investigated). It is therefore of great interest to understand better how the shallow velocity structures within the basin affect wave propagation, and how it can behave during strong shaking.

In order to provide/discuss answers to these questions, the GFZ German Research Centre for Geosciences, in cooperation with the Central Asian Institute of Applied Geosciences (CAIAG), within the framework of the Global Change Observatory Central Asia (GCO-CA) initiative of

45 the GFZ, established the Bishkek Vertical Array (BIVA) of accelerometers at the same site
46 where the seismic noise measurements were carried out by Parolai *et al*., (2010). Downhole
47 measurements are a valuable complement to *in situ* surface and laboratory geotechnical
48 investigation techniques. In fact, they provide critical constraints for both the interpretation
49 methods of surface observations as well as information about the real material behavior and
50 overall site response over a wide range of loading conditions (Assimaki *et al*. 2008). The
51 amount and quality of information from downhole arrays in seismically active areas is the
52 key to improving our understanding of *in situ* soil behavior, to assess modeling and
53 parametric uncertainties associated with employed methodologies for strong-motion site-
54 response analysis, and for shallow geological investigations.
55 In this paper we will first describe the vertical array configuration and the motivation behind
56 its establishment, and second, taking advantage of recordings of a Mb 4.7 earthquake that
57 occurred 40 km from the array site during the installation phase, we will show the results of
58 data analysis that allow us to estimate the S-wave velocity and Qs structure at the array site,
59 following the approaches outlined in Parolai *et al.* (2009; 2010; 2012). We will also show the
60 results of the nonstationary ray decomposition (Kinoshita, 2009) that allowed at least 3
61 reflectors in the shallow velocity structure below the array to be identified.

62 **2. VERTICAL ARRAY DESCRIPTION**

63 A 150 m depth borehole was drilled in the courtyard of CAIAG in Bishkek (Figure 1). The
64 borehole, cased along its entire length, crossed different Quaternary sedimentary layers
65 (Parolai *et al*., 2010 and reference therein). In particular, the uppermost 80 meters is
66 dominated by alternating layers of coarse gravel-shingle, and sandy layers with varying
67 thicknesses (Figure1), while below 80 m depth only one thick gravel-shingle layer is present.
68 The main ground water table was encountered at a depth of about 55 m. Parolai *et al.*

(2010) estimated by Rayleigh wave dispersion curve inversion that the average S-wave velocity is around 600 m/s in the uppermost 25 m, increasing to 750 m/s between 25 and 50 m depth and from nearly 1000 m/s to 1350 m/s over the next 100 m.

The borehole is equipped with a 3-component accelerometer at the surface and a chain of five 3-component borehole accelerometers at depths of 10, 25, 45, 85 and 145 m. The sensors are connected to two 24 bit digitizers. The output was set to +/- 2 g and the sampling rate in 500 samples per second (s.p.s.). The data are stored locally and transmitted in real time via the internet (after being re-sampled to 50 s.p.s.) to CAIAG and the GFZ. In case of a significant event, the 500 s.p.s data can be manually downloaded. During the installation it was possible to orient with respect to the cardinal points only the horizontal components of the sensor located at the surface.

3. THE Mb 4.7 18:03:2011 EARTHQUAKE RECORDINGS

On March 18th 2011 during the installation phase of the vertical array, an earthquake of Mb 4.7 (Mw 4.1) occurred nearly 40 km north-northeast of the array site (Figure 1) at an estimated depth of only 2 km. The earthquake was recorded by the sensors installed at 10 m, 25 m, 45 m, and 145 m depth. Unfortunately, due to malfunctions during the installation, phase recordings are not available for the sensors at 85 and 0 m depth. The recordings of the earthquake clearly show a strong arrival (at 398 s, Figure 2) before the S-wave one (at around 399 s, Figure 2). This earlier arrival is also observed in the horizontal components, although less clearly. A simple cross correlation analysis on these seismograms (not shown here) showed that this pulse is propagating at a velocity very similar to that of the direct P-wave arrival. We therefore speculate, and will show the feasibility of this idea in this paper, that this is a SP phase due to a conversion at the seismological bedrock of the basin which is

expected to be at around 3 km depth (Bullen *et al*., 2001). Considering the location of the hypocenter and the polarities of the first P-wave arrival in the vertical and horizontal components, it is possible to assess the orientation of the nominal north-south and east-west component with respect to the cardinal points (see NMSOP, 2002). In fact, knowing the position of the epicenter, it is possible to compare the observed polarities of the first arrival with the expected ones from theory, and therefore to estimate to a first order the orientation of the sensors' components in the borehole. In order to obtain the radial and transverse component seismograms, the horizontal recordings have been rotated, considering from the previously obtained information about the first order orientations, until the energy is maximized (minimized) in the signal window, including the converted SP phase, therefore determining the radial (transverse) direction.

Figure 2 shows the obtained radial and transverse component of ground motion after rotation. We note, as would be expected if this was correctly done, that the P-wave energy of the first arrival is minimized in the transverse component. Figure 3 shows the pseudo acceleration response spectra (5% damping) for the different components of ground motion at different depths. They clearly show that the variability of amplitude of ground motion at different frequencies and at different depths cannot be simply related to the impedance variation in the vertical direction.

The polarization of the SP phase (Figure 4) is consistent with that of the P-wave arrival (nearly in the vertical direction) as opposed to the S-waves, which are nearly polarized in the orthogonal direction. Note that only the first impulse is considered for all the phases in the analysis (double pulse in acceleration). The deviation from linearity of the polarization of these phases might be related to the effect of down-going waves that, due to the shallow depth of the sensors, can interfere with the direct first pulse arrival.

4. Inversion of the deconvolved wavefield spectra

The inversion of the deconvolved wavefield spectra (obtained by deconvolving the ground motion recorded at different depths with that measured by a reference accelerometer at a chosen depth) to obtain the S-wave velocity and Qs profile in the borehole was carried out. Although the inverse problem is non-linear, as shown in Parolai *et al.* (2012), it can be linearized when a suitable starting model is available, for example when using the information from the travel time propagation estimated by the borehole recordings. Since this is valid also in the case at hand, we carried out the inversion following the linear inversion scheme proposed in Parolai *et al.* (2012). The inversion was run considering SH waves and therefore only the spectra of the transverse components were used. Different inversions were carried out considering incidence angles at the bottom of the array ranging between 0° and 30°, including an angle of 17.4° which would be expected considering the hypocentral position and a 1D crustal velocity model for the area (Abdrakhmatov personal communication).

A starting model for the inversion was chosen that combined the available stratigraphic data with results obtained following the Parolai *et al.* (2010) approach, where the Fourier spectra of the deconvolved wavefield between the shallowest sensor and a borehole one (from now on also referred to as “data”) are fitted by an analytical transfer function via a grid search procedure. We should remark here that differently from the data used in Parolai *et al.* (2010), the wavefield of the 18.03.2011 earthquake was not recorded at the surface sensor of the BIVA array and the deconvolution must therefore be carried out using as the reference sensor the one located at 10 m depth. Although a preliminary examination of the spectra of the transverse component (not shown here) showed that the main effect of the down going waves is to generate a spectral trough at nearly 12 Hz (that is, at a frequency

higher than the frequency band where the effect of downgoing waves is expected to occur in the deeper borehole recordings), the low Qs in the shallowest layer and the presence of the spectral trough might also bias the spectral amplitude of the recording at 10 m at frequencies much lower than 10 Hz. This, in turn, would of course bias the deconvolved wavefield fit results if not correctly accounted for in the analytical expression of the deconvolved wavefield. For this reason, the analytical expression of the deconvolved wavefield *S*(*h,h1;f*) for the vertical propagation of S-waves, where *f* is the frequency, *h* the depth of the deepest sensor and *h1* the depth of the reference shallow sensor, had to be modified in this study, with respect to that used in Parolai *et al.,* (2010) in the following way:

$$S(h;h1;f)=\frac{\sqrt{1+e^{-4\pi f\beta}+2e^{-2\pi f\beta}\cos(4\pi ft)}}{\sqrt{e^{-2\pi f(t-t1)/Qs}+e^{-2\pi f\alpha}+2e^{-\pi f(t-t1)/Qs}e^{-\pi f\alpha}\cos(2\pi f(t-t1))\cos(2\pi f(t+t1))+2e^{-\pi f(t-t1)/Qs}e^{-\pi f\alpha}\sin(2\pi f(t-t1))\sin(2\pi f(t+t1))}} \quad (1)$$

With:

$$\alpha=\frac{(q1(t-t1)+2Qs\,t1)}{q1Qs} \quad (2)$$

$$\beta=\frac{(q1(t-t1)+Qs\,t1)}{q1Qs} \quad (3)$$

where t and $t1$ are the travel times between the depths h and $h1$ and the surface, respectively. $q1$ and Qs are the quality factors above h1 and between h and h1, respectively. The deconvolution of the transverse component wavefield was carried out using a regularized Tikhonov deconvolution approach (Tikhonov and Arsenin 1977; Bertero and Boccacci 1998; Mehta *et al.* 2007b) as in Parolai *et al*. (2010).

The grid search fit was first carried out considering the 25 m depth recordings with t, $q1$ and Qs as free parameters. In this step, it was assumed that $q1$ and Qs are equal, and we used this constraint in the grid search. While this assumption is justified by the shallow depth of both instruments, the geological profile and the estimation of very similar Vs in the uppermost 25 m from the geophysical investigation of Parolai *et al.* (2010) allows one degree of freedom to be eliminated from the inversion procedure, making the results more stable. In the following steps, the grid search was carried out considering the 45 m and the 145 m depth recordings. In these cases, $q1$ was fixed to the value obtained in the first step. The grid search was carried out in both steps with Qs values ranging from 1 to 500 over steps of 1. The t ranges and the $t1$ value were selected considering the travel time that could be estimated by examining the first spectral trough in the spectra of the recordings (Parolai *et al.* 2010) that is generated by the down going wave interference.

Note that by only including the effect of down-going waves in the shallowest depth recording (10 m), it is possible to explain the lower amplitude of the second trough with respect to the third one as in the 10m/45m deconvolution wavefield spectra (see the spectra in Figure 5). An average Qs of 5, 5, 20 and 21 were estimated for the layers between 0m-10m, 10m-25m, 10m-45m and 10m-145m, respectively, while the average Vs values estimated were 524m/s, 440m/s, 560 m/s and 950 m/s between 0m-10m, 10m-25m, 10m-45m and 10m-145m, respectively.

183 The target frequency band for the inversion was chosen to be 0.5 Hz to 10 Hz in order to
184 avoid problems due to the regularization of the spectral trough contained in the
185 denominator (which is here the spectrum of the 10 m depths recording, Parolai *et al*. 2010;
186 Parolai *et al*. 2012).

187 Figure 5 shows the results obtained considering different incidence angles of the seismic
188 waves. The lower misfit results (estimated as the root mean square of the differences
189 between the observed and the calculated data) are generally obtained for incidences close
190 to the vertical. Note that at frequencies higher than those used in the inversion, the fit is
191 also satisfactory. Although the 0° and 10° incidence models provide very similar S-wave
192 velocity profiles, they strongly differ in their Qs structure below 80 m depth. Considering
193 that the large inversion affecting the Qs value at about 80 m for the 0° incidence model does
194 not seem to be justified, neither by the available geological data nor the inferred Vs
195 structure, and that a incidence angle of 10° is consistent with what can be expected at the
196 bottom of the array due to the difference in velocity between the sedimentary layers and
197 the velocity in the bedrock (used in the 1D velocity model), we consider the best model to be
198 that derived considering a 10° incidence of the S-wave wavefield.

199 The data resolution matrix (Menke, 1989) (Figure 6, bottom), that shows how well
200 neighboring data can be independently predicted or resolved, shows that only the troughs in
201 the spectra of the deconvolved wavefield can be correctly retrieved in the inversion.
202 However, as indicated by the large values of off-diagonal elements, because of the
203 periodicity of the troughs in the spectra, part of the information is distributed to nearby
204 spectral troughs. Figure 6, top, also shows the model covariance matrices (which describes in
205 which way errors are mapped from the data to the model parameters) and model
206 resolution, (showing how reliably the model parameters can be independently resolved,

Menke, 1989) where the parameter numbers from 1 to 7 and from 8 to 14 represent the velocity and Qs of each layer, respectively. The model resolution matrix shows that the first layer of the model has a low resolution with respect to Vs and that strong trades off exist between the second and third layers, as well as between the fifth and sixth layer Vs values. However, a good resolution for Qs is shown for the uppermost six layers. These results appear in contrast to the Parolai *et al.* (2012) conclusions, where generally the Vs velocity was well constrained in the inversion while Qs suffered from a lower resolution. Indeed, in this case, the strong trade off in the uppermost layers is simply a consequence of the lack of surface recordings. In such a case, a large range of Vs values can be used to describe the Vs in the first layer under the condition that it is not generating a spectral trough due to down-going waves in the spectral band used in the inversion. Consequently, the Vs in the second and third layers simply adjust with respect to that in the first layer in order to reproduce the spectral troughs at the frequency values shown by the observed deconvolved wavefield spectra. It is also worth remarking that as with Parolai *et al.,* (2012), it seems that the number of layers might therefore be reduced, independent of the stratigraphy, to a number consistent with the number of borehole sensors. In any case, we believe that the obtained model is a good representation of the underground structure in terms of average Vs velocities. Finally, the covariance matrix (Fig. 6) shows that in the final model, the error propagation mainly affects the VS estimation (parameter number from 1 to 7).

5. Nonstationary ray decomposition

The nonstationary ray decomposition method proposed by Kinoshita (2009) was applied to the transverse component recordings in order to identify the presence of the main velocity boundaries within the sedimentary cover and at the sedimentary layer-basement system.

231 This method assumes that the unknown subsurface is a homogeneous half-space and
232 performs an inversion of the seismograms by decomposing them into up-going and down-
233 going waves. The distribution of the instantaneous power of the decomposed rays,
234 calculated for the Wigner-Ville distribution (Classen and Mecklenbrauker, 1980), is
235 represented in the (t,τ) space, where t is the lapse time and τ the depth time, and used to
236 identify possible velocity boundaries, where local maxima of instantaneous power appear at
237 the intersections of the up-going and down-going rays. The maxima of the instantaneous
238 power should be correlated with the largest impedance contrasts within the sedimentary
239 cover and at the top of the seismic bedrock.

240 Figure 7 shows that under the BIVA array, at least 3 main reflectors can be identified at
241 nearly 0.5s, 1s and 1.6 s depth time τ, respectively. We propose, in reasonable agreement
242 with the geological cross section shown in Figure 8, that these boundaries are those existing
243 within the Quaternary cover, the Sharpyldak and Chu Tertiary formations, and between the
244 sedimentary material and the Paleozoic bedrock.

245

246 **6. Results from synthetic seismograms**

247 In Figure 9, synthetic seismograms calculated using the Wang (1999) approach (and used in
248 the forward propagation part of the inversion code employed by Parolai *et al.,* 2012) show
249 the propagation of S-waves between the deepest borehole sensor and the surface by using
250 the model estimated from the inversion. Part of the energy of the up-going S-wave, when
251 reaching the first 75 m depth discontinuity between the loam and the gravel-shinkle, is
252 reflected back. The energy transmitted through the discontinuity is propagated towards the
253 surface where a down-going wave is generated. When reaching the 75 m discontinuity, the

down-going wave is both reflected back to the surface (with a change in polarity) and transmitted down to the interior of the earth. Figure 9 clearly shows that the waveforms with greatest complexities, differently from what is generally thought, are those recorded in the borehole.

Figure 10 shows the synthetic P-SV seismograms calculated after adding to the shallow geological structure a layer down to 1000 m with a Vs velocity of 1600 m/s, a layer between 1000 and 3000 m with a Vs of 2000 m/s, and below this a crustal model with Vs of 3300 m/s. In this way, although without any intention to identify by trial and error a structure that would allow the matching of synthetic arrivals with observed ones, we try to include at least two of the boundaries highlighted by the nonstationary ray analysis. The velocities of the added structure are based on the geological cross section of Figure 8 (Baeva, 1999) and the crustal velocity model used to locate earthquakes in the area (Abdrakhmatov pers. comm.). The synthetic seismograms show that such a geological structure is able to generate, consistent with the observed seismograms, a clear SP phase at the bottom (3 km) of the basin. Although the absolute velocities in the model are not perfectly resolved (the estimated delay time between the SP and S wave arrivals is different from that observed) the generation of converted waves is clear, as well as the presence of multiple reflections, consistent with the instantaneous power of decomposed ray images. Due to these encouraging results, future work, when a larger number of recordings will be hopefully available, should be devoted to retrieving details of the velocity structure.

7. CONCLUSIONS

In this study, recordings made by the BIVA vertical array recently installed in Bishkek (Kyrgyzstan) are presented. The array will offer the first opportunity to acquire digital strong

motion data at different depths in this high seismic risk area. Using the recordings of a single event by some of the borehole seismometers, we showed that even a preliminary analysis can provide interesting information about the underground structure in the basin and about the associated wave propagation.

In particular, the importance of large converted phases was identified and the existence of several velocity boundaries within the sedimentary cover assessed. This may allow us in the future to understand better the role of the geological structures in the spatial variability of hazard, and therefore risk, in Bishkek.

Refining these analyses will be the aim of future studies and, when a larger amount of data is available, a better knowledge of both the basin structure and of wave propagation within it will be possible.

Acknowledgement

We thank the associate editor J. Zahradnik, N. Mikhailova and an anonymous reviewer for comments and suggestions that helped in improving the manuscript. The figures were drawn using GMT (Wessel and Smith 1991). A. Strollo helped with the organization of the BIVA array planning and installation. R. Milkereit improved figures. Kevin Fleming kindly revised our English. This research was supported by the Global Change Observatory Central Asia of the GFZ.

296

297 **References**

298 Assimaki, D., W. Li, J. Steidl, and K. Tsuda (2008). Site amplification and attenuation via
299 downhole array seismogram inversion: A comparative study of the 2003 Miyagi-Oki
300 aftershock sequence. Bulletin of Seismological Society of America **98**, 301–33.

301 Baeva, N.B. (1999) Geological profile, Government Agency of geology and mineralogy of
302 Kyrgyz Republik. Kyrgyz-Hydro-geological expedition.

303 Bertero, M., and P. Boccacci (1998). Introduction to inverse problems in imaging, Institute Of
304 Physics, Bristol.

305 Bindi, D., M. Mayfield, S. Parolai, S. Tyagunov, U.T. Begaliev, K. Abrakhmatov, B.
306 Moldobekov, and J. Zschau (2011). Towards an improved seismic risk scenario for Bishkek,
307 Kyrgyz Republic. Soil Dynamics and Earthquake Engineering **31**, 521-525.

308 Bullen, M. E., D. W. Burbank, J. J. Garver, and K. Y. Abdrakhmatov (2001). Late Cenozoic
309 tectonic evolution of the northwestern Tien Shan: New age estimates for the initiation of
310 mountain building. Geological Society of America Bulletin **113**, 1544-1559.

311 Classen, T. A. C. M., and W.F.G. Mecklenbräuker (1980). The Wigner Distribution — a tool
312 for time frequency signal analysis, 3 parts. Philips Journal of Research, **35**, 217–250, 276–
313 300, 372–389.

314 Erdik, M., T. Rashidov, E. Safek, and A. Turdukulov (2005). Assessment of seismic risk in
315 Tashkent, Uzbekistan and Bishkek, Kyrgyz Republic. Soil Dynamics and Earthquake
316 Engineering **25**, 473-486.

317 Kinoshita, S. (2009). Nonstationary ray decomposition in a homogeneous half space, Earth
318 Planets Space, **61**, 1297-1312.

319 Mehta, K., R. Snieder, and V. Graizer (2007b). Extraction of near-surface properties for a
320 lossy layered medium using the propagator matrix. Geophysics Journal International **169**,
321 271-280.

322 Menke, W., (1989). Geophysical data analysis: Discrete inverse theory, Academic Press,

323 ISBN 0-12-490921-3.

324 New Manual of Seismological Observatory Practice (NMSOP, 2002), ISBN 3-9808780-0-7

325 Parolai, S. (2009). Denoising of seismograms using the S transform. Bulletin of Seismological
326 Society of America **99**, 226-234.

327 Parolai, S., R. Wang, and D. Bindi (2012). Inversion of borehole weak motion records
328 observed in Istanbul (Turkey). Geophysics Journal Internation **188**, 535-548.

329 Parolai, S., S. Orunbaev, D. Bindi, A. Strollo, S. Usupaev, M. Picozzi, D.D. Giacomo, P.
330 Augliera, E. D'Alema, C. Milkereit, B. Moldobekov, and J. Zschau (2010). Site effects
331 assessment in Bishkek (Kyrgyzstan) using earthquake and noise recording data. Bulletin of
332 Seismological Society of America **100**, 3068-3082.

333 Tikhonov, A. N.,and V. Y. Arsenin (1977). Solutions of Ill-Posed Problems, Winston and Sons,
334 New York, ISBN 0470991240

335 Wang, R. (1999). A simple orthonormalization method for stable and efficient computation
336 of Green's functions. Bulletin of Seismological Society of America **89**, 733–741.

337 Wessel, P., and W. H. F. Smith (1991). Free software helps map and display data, Eos Trans.
338 AGU 72, **41**, 445–446.
339
340 Zhang, P., Z. Yang, H. K. Gupta, S. C. Bhatia, and K. M. Shedlock (1999). Global seismic hazard
341 assessment program (GSHAP) in continental Asia, Annali di Geofisica **42**, 1167-90.
342

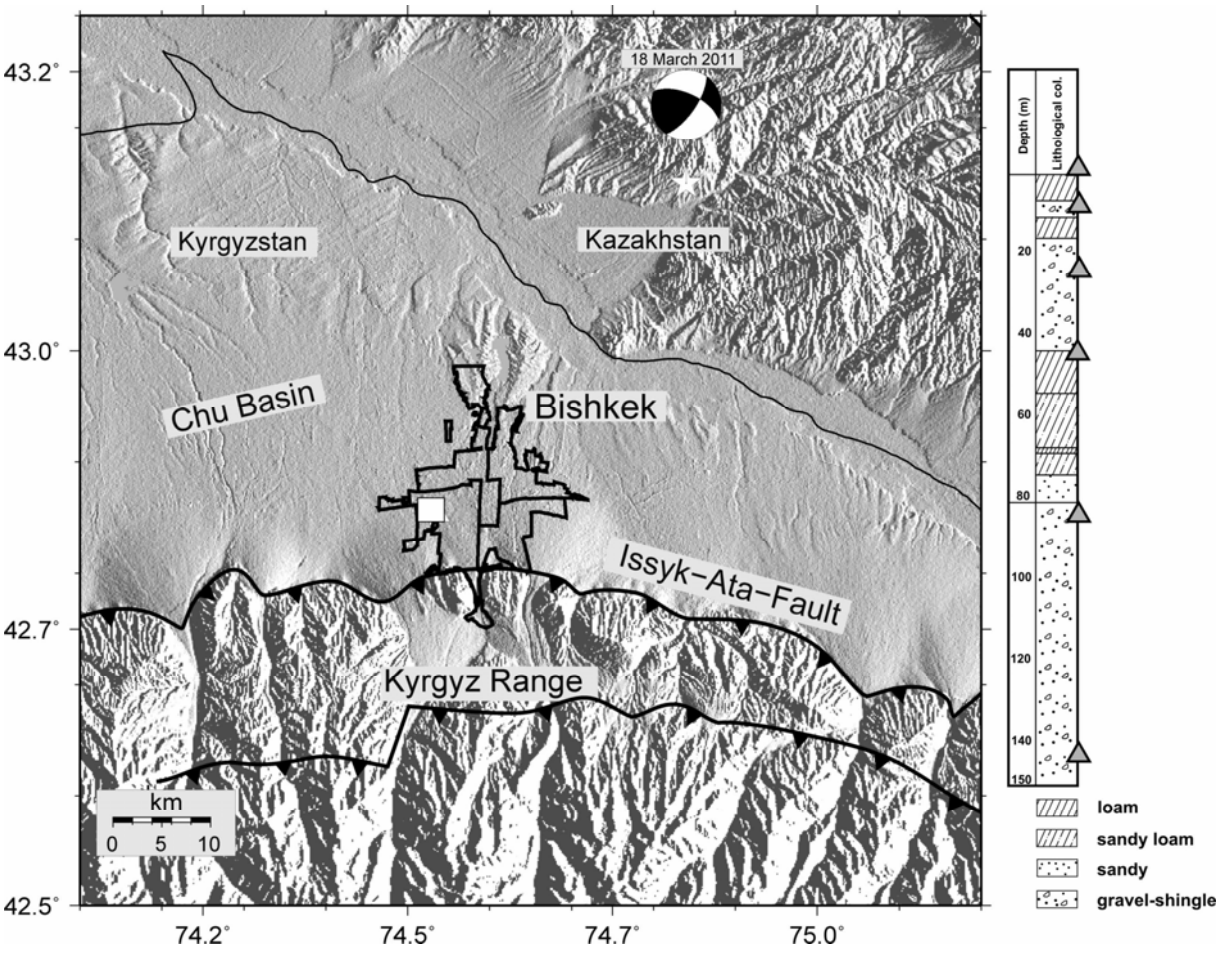
18 March 2011
Kyrgyzstan
Kazakhstan
Chu Basin
Bishkek
Issyk−Ata−Fault
Kyrgyz Range
km
0 5 10
43.2°
43.0°
42.7°
42.5°
74.2°
74.5°
74.7°
75.0°
Depth (m)
Lithological col.
20
40
60
80
100
120
140
150
loam
sandy loam
sandy
gravel-shingle

Figure 1.

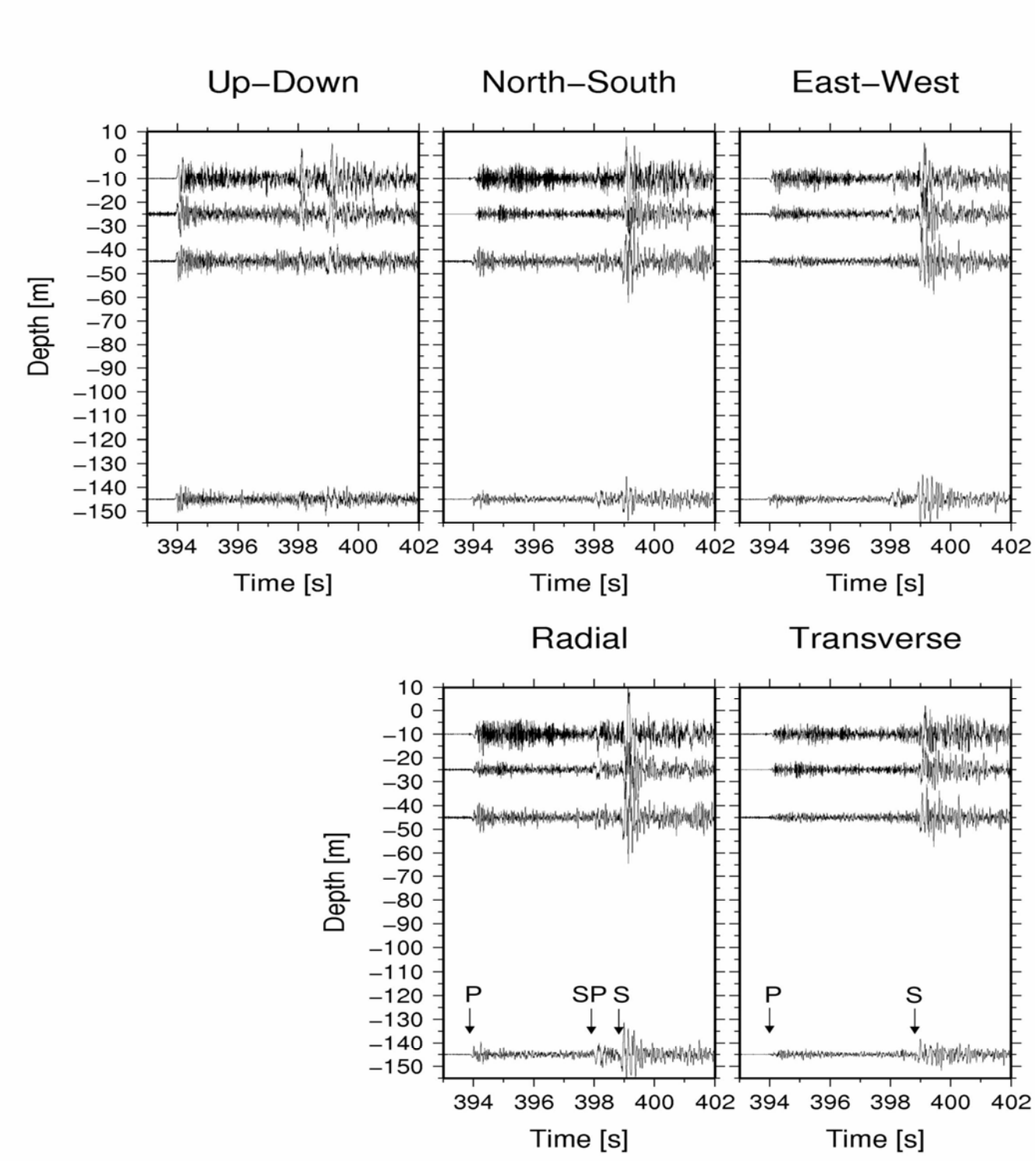

348

349 **Figure 2.**

350

351

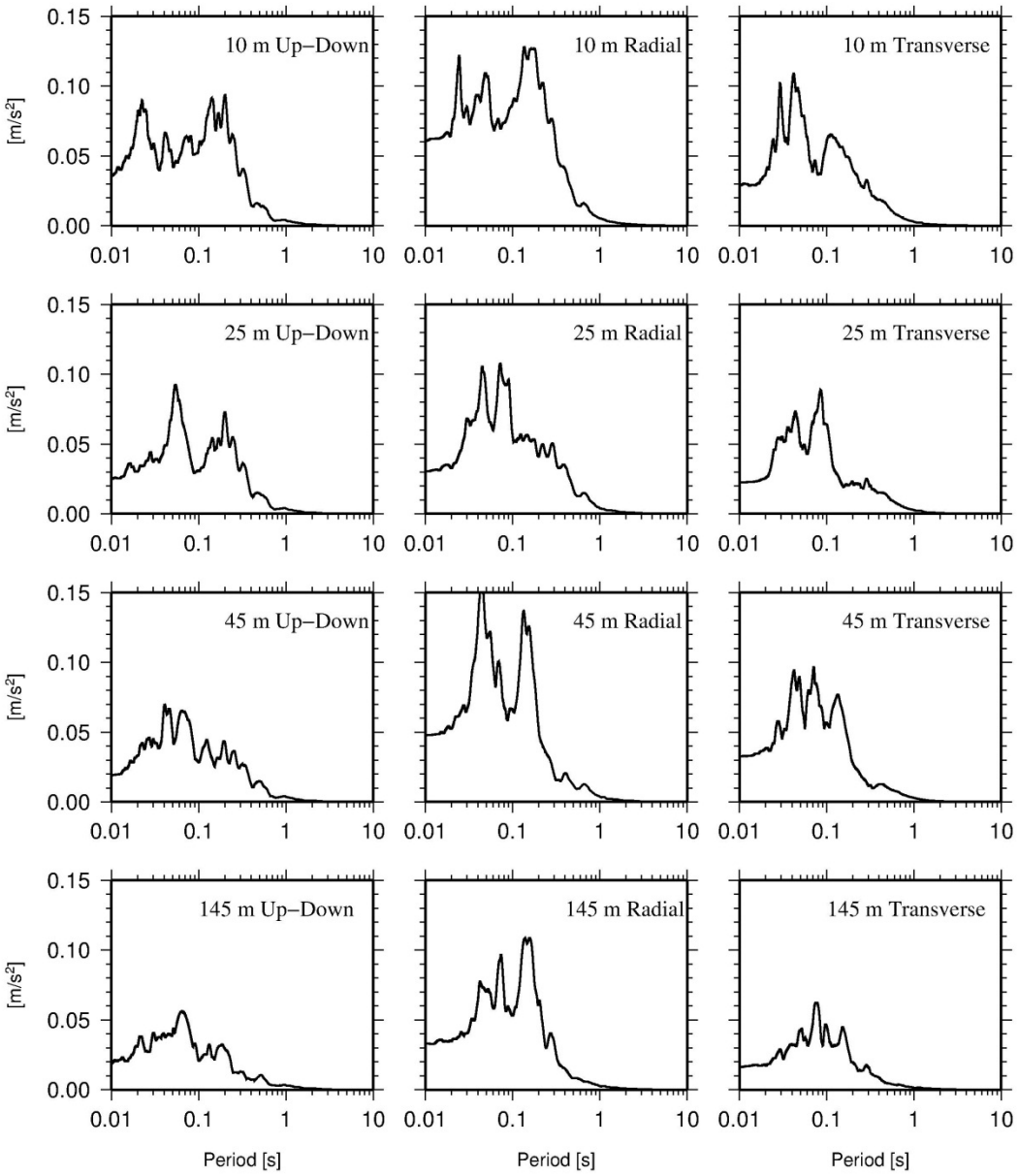

352

353 **Figure 3**

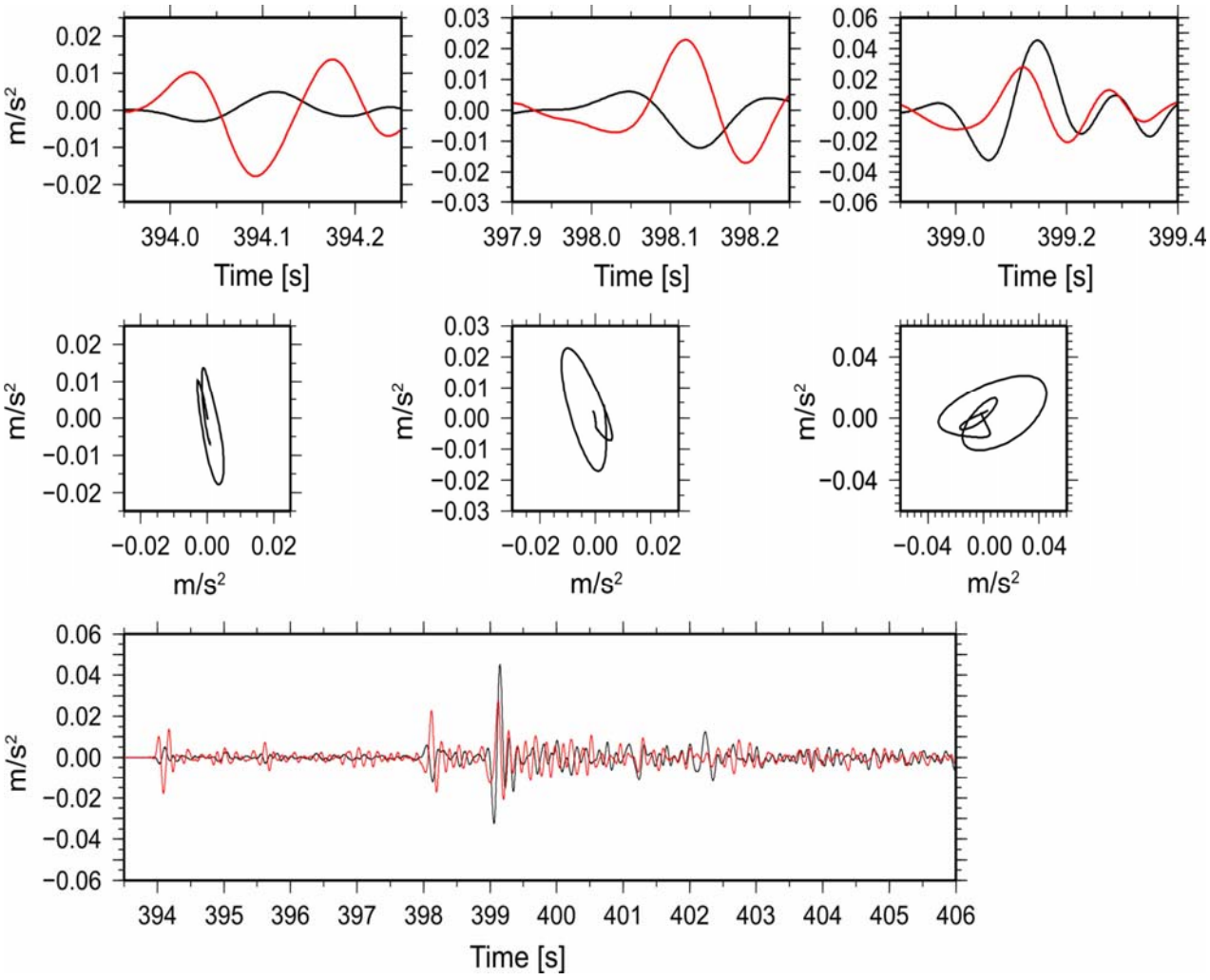
m/s²
Time [s]
394.0
394.1
394.2
397.9
398.0
398.1
398.2
399.0
399.2
399.4
394
395
396
397
398
399
400
401
402
403
404
405
406

Figure 4.

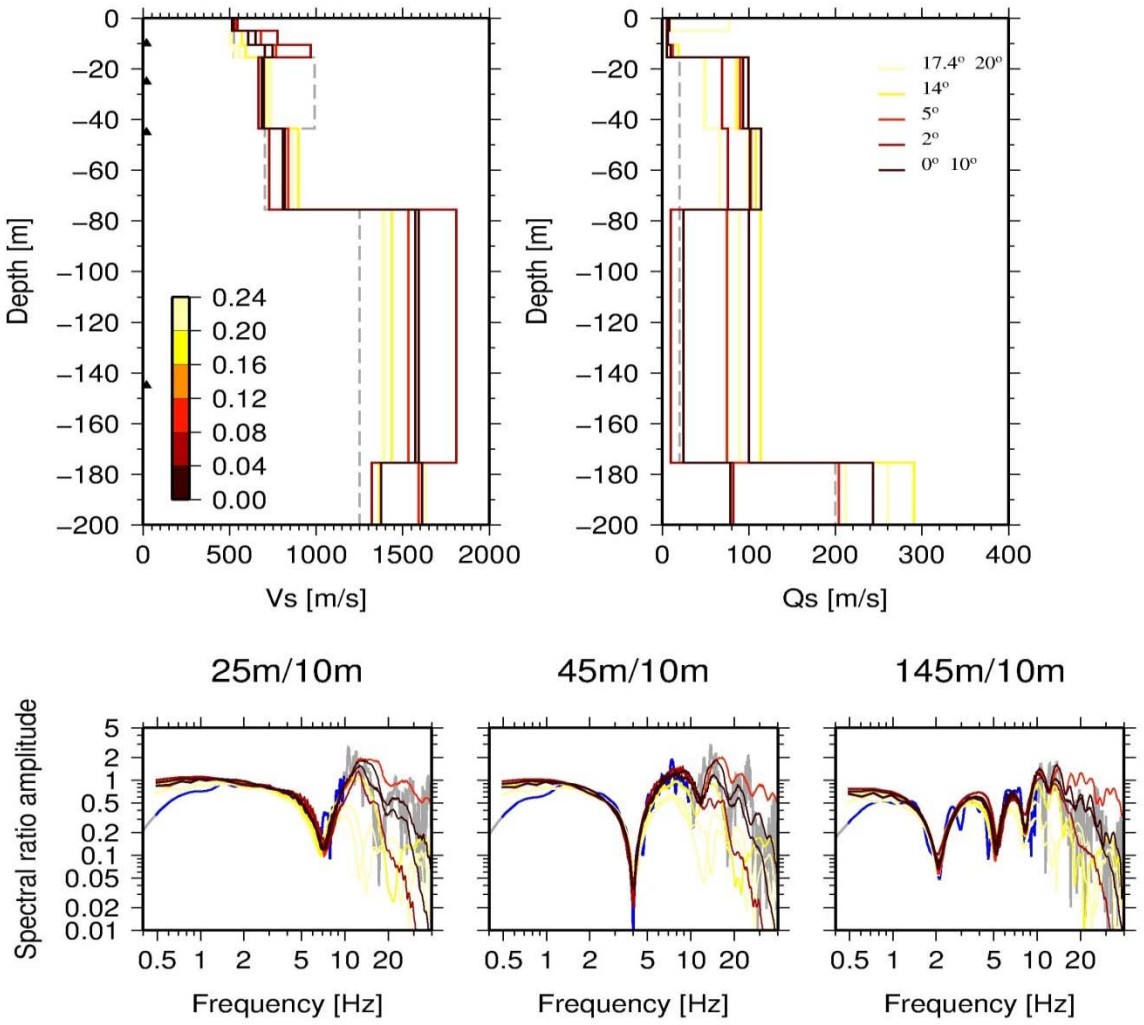
Depth [m]
Vs [m/s]
0.24
0.20
0.16
0.12
0.08
0.04
0.00
Qs [m/s]
17.4° 20°
14°
5°
2°
0° 10°
25m/10m
45m/10m
145m/10m
Spectral ratio amplitude
Frequency [Hz]

Figure 5.

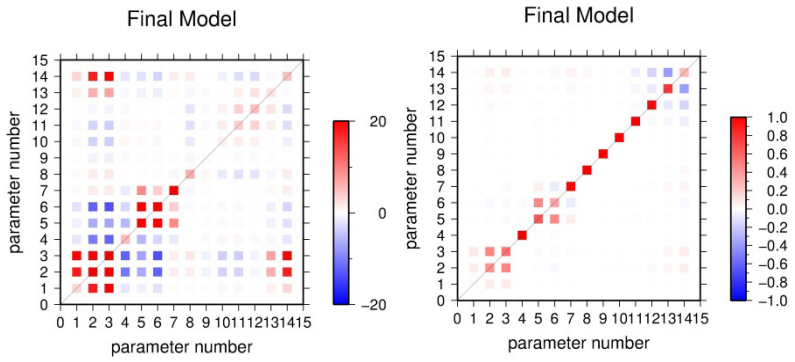

362

363

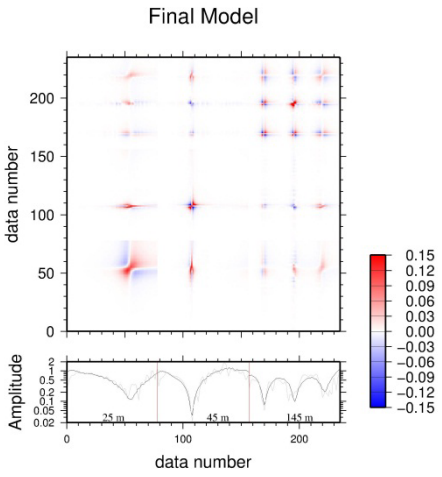

364

365 **Figure 6.**

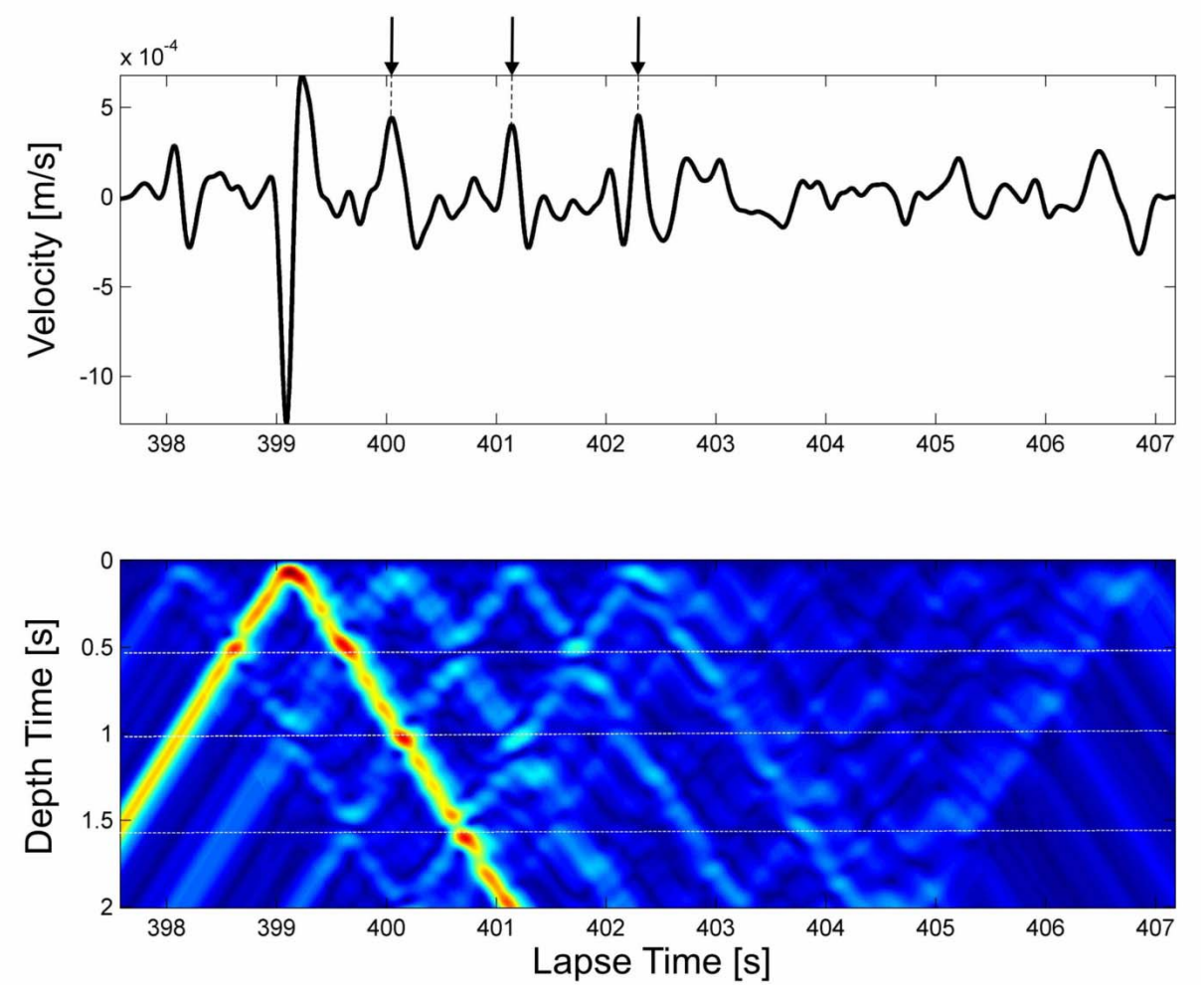

366

367 **Figure 7.**

368

369

370

371

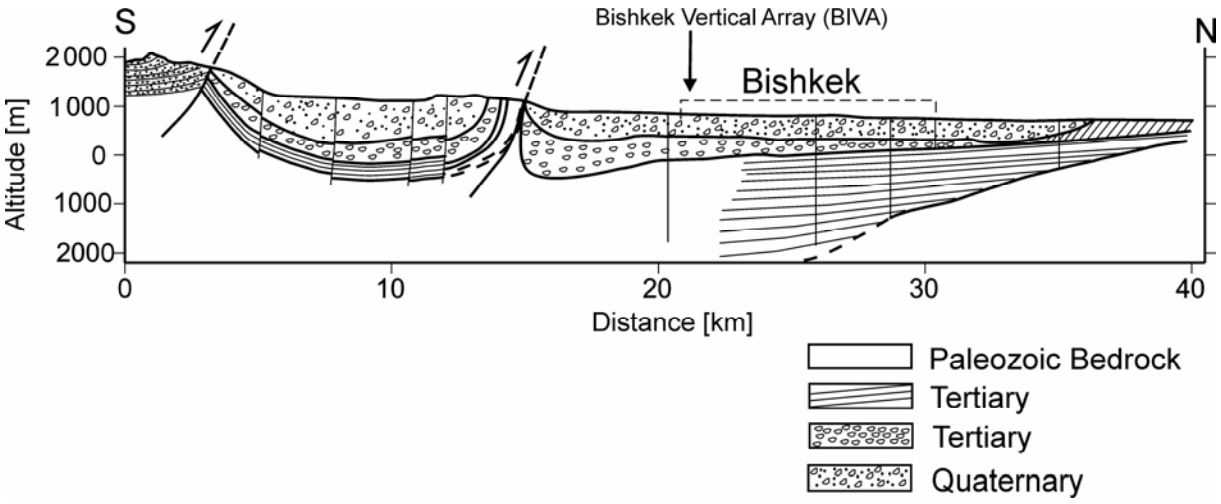

372

373 **Figure8**.

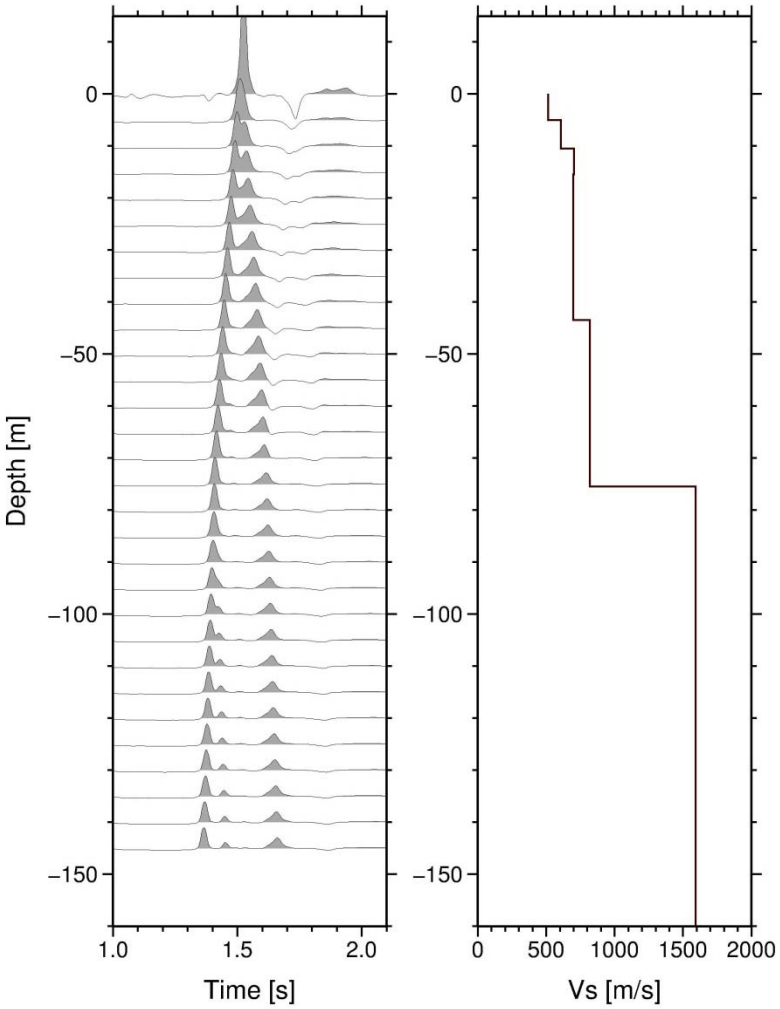

374

375 **Figure 9**.

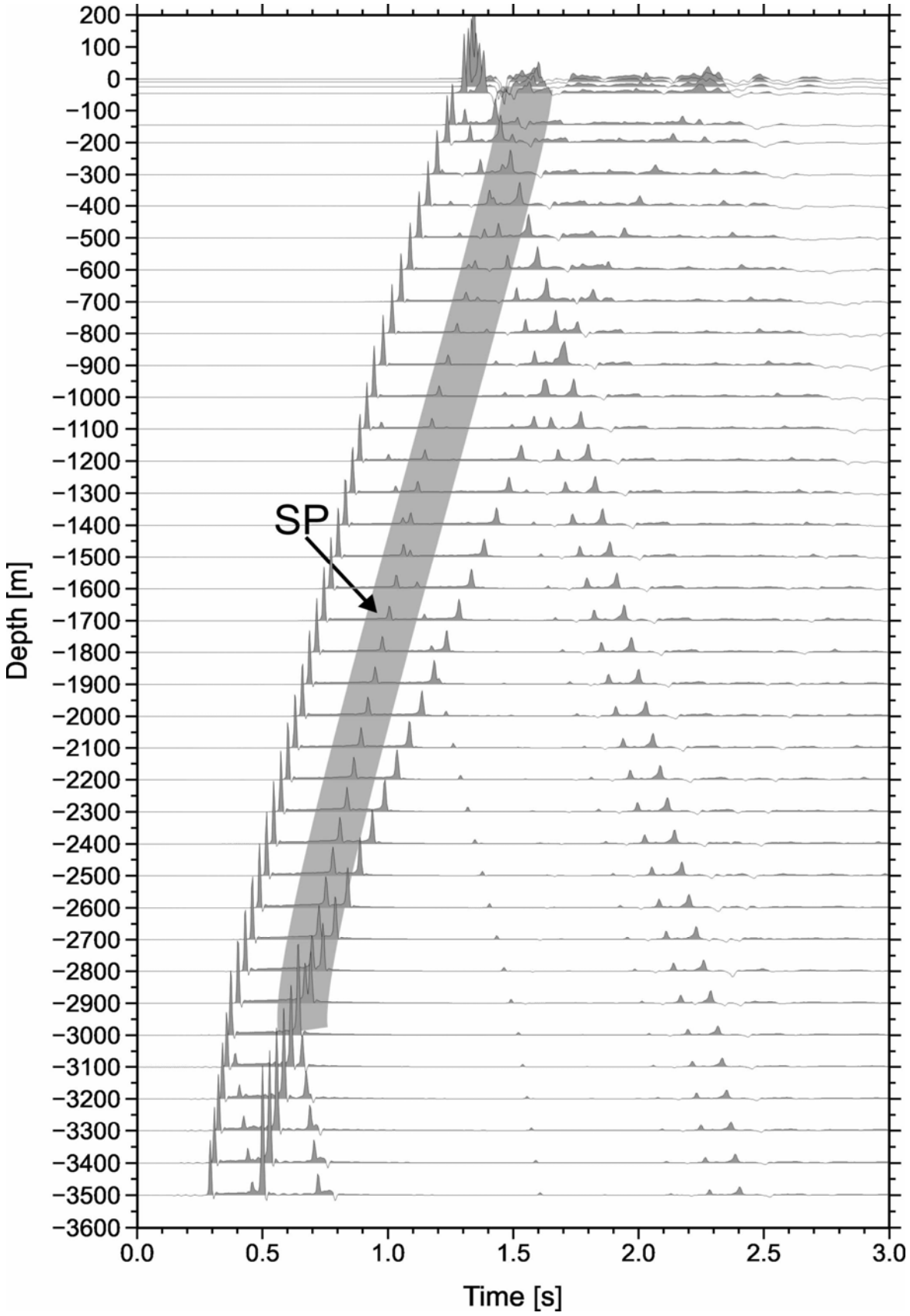

376

377 **Figure 10**.

Figure 1: Map of the area under investigation. The white square indicates the position of the vertical array. The focal mechanism of the 18 March 2011 earthquake is depicted at the epicenter position. The BIVA vertical array stratigraphic column is shown to the right.

Figure 2. Top panels: Horizontal and vertical ground accelerations recorded at different depths. Bottom panels: Radial and transverse components of acceleration of ground motion obtained after rotation. The P, SP and S phase arrivals are indicated.

Figure 3. The 5% damping pseudo-acceleration response spectra for the different components of ground motion at different depths.

Figure 4. Top panels: (From left to right) The signal windows used for the polarization analysis of the P, SP and S-waves recorded at 10 m depth. Black is the vertical component of acceleration, red the radial one. Middle panels: (From left to right) the polarization of the P, SP, and S-waves. The horizontal axis indicates the radial component, the vertical axis the vertical one. Bottom panel: The vertical and radial components of the acceleration at 10 m depth after low pass filtering (10 Hz).

Figure 5. Top left hand panel: the best fitting Vs models obtained after the inversion of the spectra of the deconvolved wavefield. Different colors indicate different degrees of fit obtained for different incidence angle of the wavefield. The dashed gray line indicates the

399 starting model of the inversion. Top right-hand-panel: The same as for the left, but for Qs.
400 Bottom panels: Observed (gray line) and calculated (color lines) deconvolved wavefield
401 spectra for the best fitting. The blue line indicate the frequency band used in the inversion.
402 Different colors indicate the different degree of fit obtained for different incidence angle of
403 the wavefield.
404
405 **Figure 6.** Top left-hand panel: Model covariance matrix . Top right-hand panel: Model
406 resolution matrix . Bottom : Data resolution matrix and observed and calculated data. All
407 the matrices are for the best fit final model.
408
409 **Figure 7.** Top: Transverse component velocity time history at 10 m depth. Arrows indicate
410 the reflected waves. Bottom: Instantaneous power of the decomposed rays in the (t, τ)
411 domain, where t is the lapse time and τ the depth time.
412
413 **Figure8**. The north-south geological cross-section of the Bishkek basin redrawn after Baeva
414 (1999).
415
416 **Figure 9**. Left-hand panel: Synthetic seismogram for SH waves propagating in the estimated
417 Vs velocity structure. Right-hand panel: the Vs velocity structure.
418
419 **Figure 10**. Synthetic seismograms showing the propagation of the P-SV wavefield in the
420 approximated geological structure below the BIVA array. The gray area indicates the SP
421 converted phase.